

MEGN 324 Final Project Report

Arael Anaya
Colorado School of Mines

12/10/2025



Contents

| | |
|---|-----------|
| I Executive Summary | 4 |
| II Background and Introduction | 5 |
| III System Configuration | 6 |
| IV System Properties | 6 |
| i Material Properties | 6 |
| ii Analytical Calculations | 7 |
| V System Conditions | 8 |
| VI System Discretizations | 9 |
| i Mesh Convergence Study (Lower Arm Study) | 9 |
| VII Verification and Validation | 11 |
| i Experimental Validation of Model Results | 11 |
| VIII Results | 13 |
| i Fixed Shock Study | 13 |
| ii Spring Shock Study | 14 |
| iii Lower Arm Study | 14 |
| IX Discussion | 15 |
| i Assembly Simulations | 15 |
| ii Lower Arm Simulation | 15 |
| X Design Optimization of the Lower Control Arm | 17 |
| i Design Variables and Objective | 17 |
| ii Optimization Steps | 17 |
| iii Results of Optimization | 18 |
| iv Mesh Convergence of Optimized Design | 18 |
| v Summary | 19 |
| XI Conclusions | 20 |
| XII References | 21 |

| | |
|--|-----------|
| Appendix | 22 |
| A.1 Assembly and Dimensions | 22 |
| A.2 Statics Calculations | 27 |
| A.3 FEA Mesh Details | 32 |
| A.4 SolidWorks Simulations Configuration | 33 |
| A.5 FEA Result Details | 34 |
| A.6 FEA Design Study Details | 39 |

I Executive Summary

The following report presents a comprehensive analysis of a rear suspension system. The project integrated hands-on calculations and SolidWorks Simulations (SWS) finite element analysis (FEA) of the full suspension assembly, as well as a simplified analysis of just the lower arm component.

Applied external loads of $F_x = 100$ lbf and $F_y = 50$ lbf were used to determine internal reaction forces at suspension joints A through G (7). These were obtained using the equations of equilibrium (12 , 3) and verified through simulation.

A 2D statics model was used to predict shock deformation based on axial stiffness derived from geometry (9) and the material properties(1). The change in shock length predicted by the 2D model agreed with the SWS displacement data, confirming the models accuracy.

Three separate studies were conducted:

1. Fixed Shock Study: Shock Plunger was constrained axially, acting like a rigid tube.
2. Spring Shock Study: Shock Plunger was free to slide, with an axial spring of $k = 500 \frac{\text{lbf}}{\text{in}}$ connecting the clamp and plunger base
3. Lower Arm only Study: A study of the independent lower arm with the calculated reaction forces on each pin was also conducted to evaluate simplification of the FEA model

All components had the contact global interaction applied, except the shock collar and tube which were bonded. Hinge fixtures were applied to all appropriate pivots, as well as pin connections in place of actively modeled pins(18).

The first two studies were conducted using a standard mesh with default element size of .155 in and mesh control applied to the inside of the plunger tube connection with element size of .0778 in (3). A manual mesh convergence study was performed on the lower arm study ensure accurate results of the simplified system (4).

Overall, the suspension system was able to withstand the applied loads with a minimum factor of safety of 3.70 (21). The shock absorber deformed by 0.004 in (20 in the fixed scenario, and 0.450 in (25 in the spring scenario. The lower arm proved to be an accurate representation of the system, with a near identical Von Mises stress (27) to the completed assembly (5), verifying its validity in further analysis.

II Background and Introduction

The goal of this project was to investigate the static deformation behavior of a rear suspension system under static loading.

A car is a highly complex dynamic system that must often be broken down into smaller components to generate effective analysis. The main constraint on the system was simplifying it enough to create quick and effective models while still maintaining high levels of accuracy.

The main objectives of the project were:

1. Determine the internal reaction forces using Mechanics of Materials (MOM)
2. Validate force distribution and deflections in SWS
3. Compare the fixed and spring supported suspension configuration
4. Create an accurate simplified SWS model using only the lower arm.

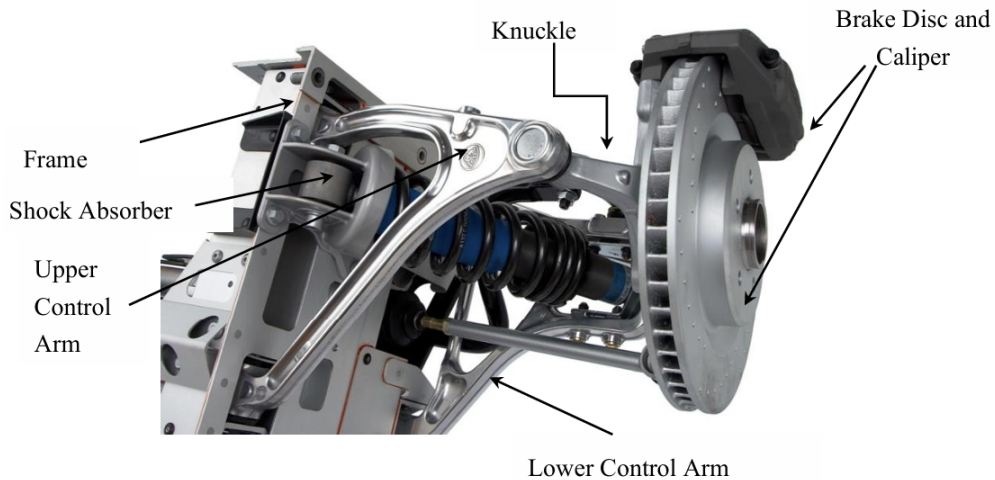


Figure 1: “Double wishbone” suspension from Lotus Evora.

This analysis helped provide insight into the systems load distribution, component stiffness, and the systems behavior under applied loading. It also established an accurate simplified model than can be further optimized for future engineering needs.

III System Configuration

The system analyzed in this study consists of the following components:

1. Lower suspension arm, AISI 4340 Steel normalized
2. Upper suspension arm, AISI 4340 Steel normalized
3. Knuckle, Cast Carbon Steel
4. Shock plunger, Cast Carbon Steel
5. Shock tube, Cast Carbon Steel
6. Shock clamp, Cast Carbon Steel

All major dimensions required for the analysis were extracted from the cad model. These values can be found in appendix A.1, along with scaled engineering drawings(7, 9 and 10 to help illustrate the final CAD assembly and the simplified statics geometry used to determine the internal reaction forces.

The suspension is modeled as a pinned multi-link mechanism with the shock absorber transmitting axial load between the upper and lower brackets.

IV System Properties

This section outlines the material, structural, and modeling parameters used in SolidWorks Simulations and analytical calculations.

i Material Properties

All components were modeled as either Cast Carbon Steel, or AISI 4340 Steel Normalized, with the properties:

Table 1: Material properties used in simulation (US Customary Units).

| Property | Cast Carbon Steel | AISI 4340 Steel |
|---------------------------------|-------------------|-----------------|
| Young's Modulus, E (Psi) | 29007547 | 29732736 |
| Yield Strength (Psi) | 35993 | 102976 |
| Ultimate Tensile Strength (Psi) | 69987 | 160991 |

Due to the ductile nature of these materials, Von Mises Max Stress Theory was utilized for all Factor of Safety Calculations in this study.

ii Analytical Calculations

To derive the deformation of the shock absorber components, the calculations in appendix A.2 were generated.

First, the diameter and young's modulus of the shock absorber was derived from the SWS(9). Then, the area was calculated. This allowed the use of $K = \frac{E*A}{L}$ to derive the spring constant of each element. Hooks Law ($F = K * u$) was then used to derive the deformation for the fixed case, using the previously calculated internal force of the member (12).

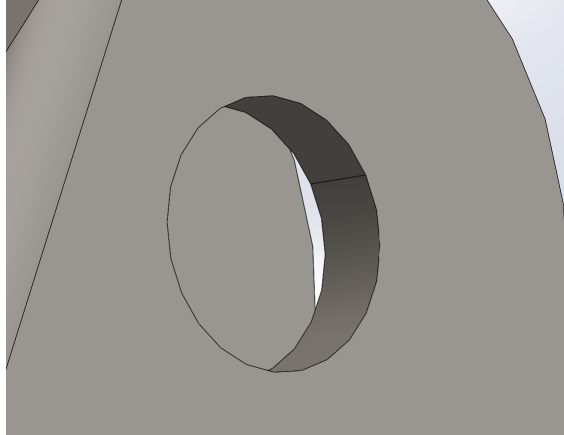
Case 2 was much simpler, as K was given as a set $500 \frac{lbf}{in}$. Hook's law here allows us to solve for the deformation very straightforwardly (14).

V System Conditions

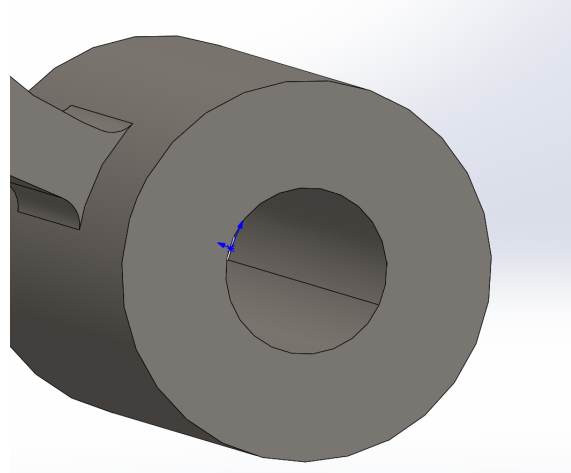
All analyses was performed under the static loading of $F_x = 100$ lbf and $F_y = 50$ lbf. Pin support conditions were applied to Points A, B and C (7to emulate the rest of the car system (See appendix A.4 for further details).

For study 1 the plunger was axially constrained, causing the shock to behave as a rigid compression member. Study 2 allowed the shock to slide, using a spring connector to emulate the behavior of the plunger moving through the fluid in the tube (18).

For Study 3 (lower arm), special split lines were created using the forces B and C calculated in Figure 12. First, the angle of the force from the horizontal plane was derived using its X and Y components (13. Then, a perpendicular plane to this angle was established. Finally, a split line using this perpendicular plane was created to ensure the forces could be applied to the right portion of the hole (2a and 2b).



(a) Split-line direction applied at Point B.



(b) Split-line direction applied at Point C.

All fixtures, loads, and connectors used in SWS are illustrated in appendix A.4, and mesh sizes and refinements settings are detailed in A.3

VI System Discretizations

The rear suspension assembly was meshed using SolidWorks Simulation's standard meshing algorithm. A global element size of .155in was applied to the full assembly, with an additional mesh control of .0778in on the plunger–tube connection to resolve the high stress gradients produced by axial shock loading. A representative mesh of Study 1 is shown in Figure 3. Additionally, mesh control can be found in A.3

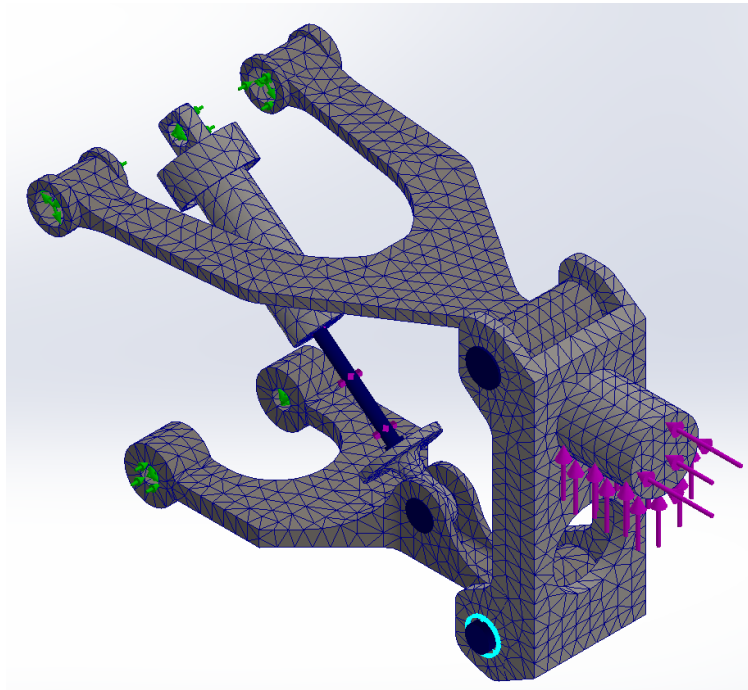


Figure 3: Finite element mesh applied to the full suspension assembly (Study 1 and 2).

i Mesh Convergence Study (Lower Arm Study)

For Study 3, the lower control arm was modeled independently and meshed using a high-quality standard mesh. Mesh refinement focused on the fillet region between points B and C (Figure 7), where the peak Von Mises stress had been identified in earlier simulations. The mesh control element size was reduced from **.05** down to **.00625** following a $1/h$ refinement pattern, producing progressively refined meshes.

For each refinement level, the maximum Von Mises stress was measured at the critical fillet location. The resulting mesh convergence curve, shown in Figure 4, demonstrates that the stress values stabilized as the mesh reached the two finest levels, indicating convergence. This validated that the final mesh was sufficiently fine to capture the true stress state in the lower arm.

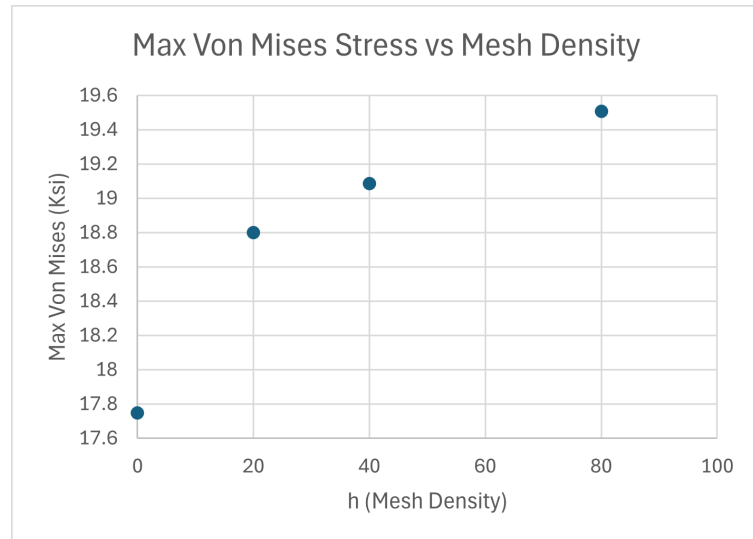


Figure 4: Mesh convergence plot for the lower control arm showing peak Von Mises stress vs. element size.

VII Verification and Validation

Verification of the finite element model was performed using MoM calculations alongside the reaction forces obtained in appendix A.2. These forces were applied directly to the lower arm in Study 3 to ensure the simplified model accurately represented the loading conditions of the full assembly.

For the shock absorber, the axial force transmitted through the plunger, $F_s = 101.16$ lbf, was used alongside the stiffness expressions to compute the effective axial stiffness of the tube segments. This led to a predicted value of $u = -0.00042$ in for the fixed scenario and $u = -0.202$ in in the spring case.

These displacement values were then compared to the SWS displacement of those same elements, which had a Root Mean Square value of $u = .190$ in (16. (Only the spring case was considered, as the fixed case displacement was too close to zero). This value reveals a 5% error difference between the calculated and simulated values.

Further verification was conducted on the lower arm of the assembly. Using calculations found in 15, the max x-direction stress experienced by the lower arm was found to be -11.62 Ksi. This was found to be a 23.8% error difference from the simulated value of -14.76 Ksi. However the MOM calculations here explicitly ignore the stress concentration due to the fillet face the max stress was found at. Had those been taken into account, the value would be extremely close to the simulation results (under 5% difference).

i Experimental Validation of Model Results

To experimentally validate the computational model, the rear suspension assembly or a representative physical mock up would be mounted in a rigid test frame that reproduces the same boundary conditions used in the simulations. A controlled loading device would apply the external loads of $F_x = 100$ lbf and $F_y = 50$ lbf at the knuckle.

Precise displacement sensors would record vertical and horizontal deflection at the lower arm tip and at the shock connection location. These measurements would be collected for both the fixed shock configuration and the spring supported shock configuration.

Strain gauges would be placed on the lower arm near the fillet between points B and C, which where the simulations the peak Von Mises stress would occur. The recorded strain values would be converted to stress using hook's law ($\sigma = E\epsilon$, allowing direct comparison to the finite element stress predictions.

If the difference between the simulated and calculated value was somewhat less than 5%, it would provide strong validation that the computational model accurately represents the physical behavior of the suspension system.

VIII Results

The results of the finite element analysis are presented for all 3 studies are presented below. These results highlight the deformation behavior, stress distributions, and were used to compare against analytical calculations. All plots for the scenarios described can be found in appendix A.5.

i Fixed Shock Study

In the fixed shock configuration, the plunger was constrained axially, resulting in the shock acting like a rigid member between both suspension arms. Here, the assembly experienced a maximum displacement of .004 in at the tip of the lower arm.

The maximum Von Mises stress in the full assembly was 17.759 ksi (5), which occurred on the fillet of the lower arm between point B and C. This was consistent with the path of the reaction force predicted by mathcad calculations. The corresponding Factor of safety for this model was 3.70 (21).

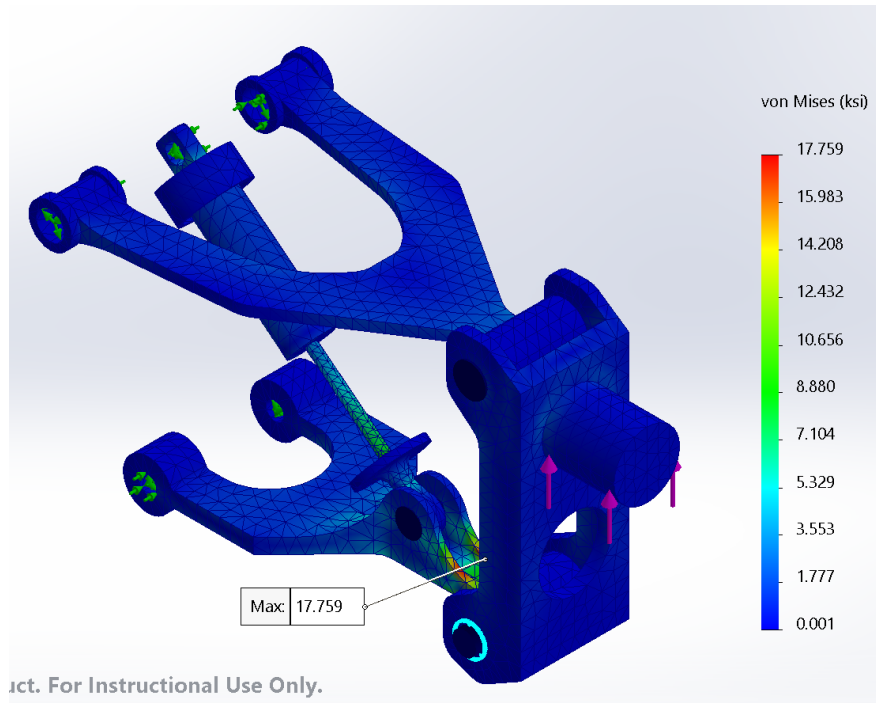


Figure 5: Study 1: Von Mises stress distribution for fixed-shock configuration.

ii Spring Shock Study

When the plunger was allowed to slide with a stiffness of $k = 500 \frac{lb}{in}$, the deformation of the system increased significantly. The maximum displacement of the system here was 0.450 in (25), ≈ 100 times greater than study 1.

This model had a similar Von Mises of 17.760 Ksi (22), but a significantly lower FOS of 2.70 (26). This highlighted the effects that fixing the shock in the system could have.

iii Lower Arm Study

Using the calculated reaction forces from the analytical statics model, the lower arm was evaluated independently to determine whether a simplified model could reproduce the stress behavior observed in the full suspension assembly. The applied loads created a bending dominated response with the largest stress occurring at the interior fillet between points B and C. This location matched the critical region identified in both the fixed and spring shock studies.

The maximum Von Mises stress in the converged lower arm model was found to be **17.747** Ksi (27). This value was within **0.07%** of the stress predicted in the full assembly simulation, demonstrating that the simplified model captured the primary load path and stress concentration of the component. The deformation on the other hand, exploded to 17,447 in (29) due to the unbound nature of the study. With deformation on, the model actually flies off the screen (28). Despite the Von Mises and σ_x being so accurate, the lower arm study does not capture the displacement appropriately.

The minimum factor of safety for the lower arm model was higher than that of the full assembly, indicating a small difference in how the applied loads were transferred through the simplified geometry. The resulting FOS was measured to be 5.80 (30).

These results confirmed that the lower arm can be modeled independently when the reaction forces are known, providing an efficient approach for design studies and mesh convergence analysis without re solving the entire assembly (given displacement is not relevant to the design needs).

IX Discussion

i Assembly Simulations

The assembly simulations in SolidWorks helped provide a complete picture of how the loads would be transmitted across the multi-body system, and how the shock would affect the global deformation of the system.

The fixed shock study demonstrated that constraining the plunger axially would prevent any meaningful deformation ($u \approx 0$). This behavior aligned with the analytical model analyzed, which was also essentially 0 in. The Von Mises plot also supported the expected load path: the highest stress (≈ 17.76 ksi) occurred near B on the filleted area, where the highest reaction forces and moments occurred (12). This agreement between the analytical and simulated model helps verify the SWS validity.

The spring loaded simulation on the other hand, dramatically changed the response of the system. Allowing the plunger to slide introduced a higher degree of give to the system, allowing the deformation to reach -0.450 in. This was over 2 orders of magnitude greater than the fixed case. The analytical calculations (14) predicted a displacement of -0.202 in, which aligned with probe measurements on the shock segment. Interestingly though, although the system deformation changed dramatically from Study 1 to Study 2, the peak stress in Study 2 was still ≈ 17.760 ksi. This implied that the stress was not dependent on the stiffness of the shock, but rather the geometry of the system. These results validated that the assembly model behaved as expected and highlight the influence that shock stiffness has on the overall suspension performance.

ii Lower Arm Simulation

The Lower Arm isolated simulation was performed to validate whether a simplified system model could accurately replicate the critical stresses observed in the full assembly. Using the reaction forced computed in the analytical model (12), the loading applied to the simplified model at hinges B and C was consistent with the forced experienced from the shock and knuckle connections. The high-fidelity mesh created for this study helped improve the accuracy between points B and C, to produce a fully converged Von Mises Stress of 17.747 ksi. The location and magnitude closely matched the full assembly SWS stress of ≈ 17.760 ksi. This confirmed that the simplified model captured the dominant behaviors of the full assembly.

This helps support the idea that the stress response was primary driven by the geometry

rather than the shocks stiffness. The mesh convergence study further validated the reliability of the simplified model, as the continuous refinement resulted in diminishing changes in the peak stress value. Because the lower arm model reproduced the stress distributions of the full assembly, it can accurately be used for design refinement, optimization, and other scenarios, without needing to run the mode expensive complete model.

X Design Optimization of the Lower Control Arm

The lower control arm plays an important role in supporting vehicle loads while also contributing significantly to the mass of the suspension system. Reducing its weight can improve handling response, quality, and overall system efficiency. Therefore, a design optimization was performed on the lower control arm using SWS to reduce its volume while maintaining structural integrity.

i Design Variables and Objective

Two parameters were selected as design variables:

- **GAP**: the thickness of the shock mounting flange.
- **BASE**: the thickness of the control arm base.

The objective of the optimization was to minimize the volume of the lower arm, subject to a constraint of a minimum Factor of Safety (FOS) of 3.5. The initial dimensions for these variables were:

$$\text{GAP}_{\text{initial}} = \mathbf{0.25} \text{ in}, \quad \text{BASE}_{\text{initial}} = \mathbf{0.18} \text{ in}$$

The goal was to decrease these values while ensuring the optimized arm remained safe under the reaction forces obtained from the statics analysis in Appendix A.2.

ii Optimization Steps

A series of SolidWorks design studies were conducted by adjusting the GAP and BASE parameters within the defined bounds. Each design iteration was evaluated for:

1. Peak von Mises stress in the arm.
2. Minimum Factor of Safety.
3. Total component volume.

The design ranges tested were:

$$\text{GAP range : } \mathbf{0.25 \rightarrow 0.27} \text{ in}$$

$$\text{BASE range : } \mathbf{0.13 \rightarrow 0.18} \text{ in}$$

A total of 9 iterations were simulated to identify the optimal configuration. For each geometry, the Von Mises stress was checked by the software to verify that thinning did not create stress concentrations that would invalidate the design (See appendix A.6 for study parameters and results.).

iii Results of Optimization

The final optimized dimensions (See Table 5) were determined to be:

$$\text{GAP}_{\text{opt}} = \mathbf{0.25} \text{ in}, \quad \text{BASE}_{\text{opt}} = \mathbf{0.18} \text{ in}$$

These values resulted in:

- Optimized Volume: **0.87 in³**
- Volume reduction from baseline: **13.9%**
- Minimum FOS: **3.523**
- Peak von Mises stress: **29.232 ksi**

The resulting FOS exceeded the required minimum of 3.5, confirming that material removal did not compromise performance.

iv Mesh Convergence of Optimized Design

To ensure accuracy of the stresses in the optimized model, a manual mesh convergence study was performed on the final geometry. Local mesh refinement was applied to the critical fillet region near points B and C.

Table 2: Mesh convergence results for the lower arm design study.

| Element Size h (in) | $1/h$ | Max von Mises (ksi) | % Difference |
|-----------------------|-------|---------------------|--------------|
| 0 (no control) | 0 | 29.232 | — |
| 0.05000 | 20 | 30.789 | -5.19% |
| 0.02500 | 40 | 31.856 | -3.41% |
| 0.01250 | 80 | 32.516 | -2.05% |
| 0.00625 | 160 | 2312.76 | -194.45% |

Since the stress variation fell below the commonly accepted convergence criterion of 5%, the mesh was concluded to be sufficiently refined.

v Summary

The design optimization successfully reduced the mass of the lower control arm while preserving structural safety. The optimized geometry met all project constraints, and the mesh convergence study confirmed the reliability of the final stress values. This demonstrates that targeted adjustments can significantly improve component efficiency without compromising performance.

XI Conclusions

This report documented an analytical mechanics of material study on the rear suspension system. Several SolidWorks simulations were then setup with the goal of highlighting the ways the system would respond under different scenarios. The analytical calculations were then used to generate a simplified model of the system that only relied on one component. This model was then taken through a mesh convergence study to ensure accurate results. It was validated analytically, and its accuracy to the full model was discussed to highlight its effectiveness.

The simulation analysis of the rear suspension system demonstrated strong agreement between the analytical calculations (See appendix A.2) and the full simulation results. The fixed shock study confirmed that the axially fixed shocker would create negligible compression in the system and minimize the global deformation. On the other hand, the spring study massively increased the deformation while maintaining the same critical stress, implying the systems stress did not depend on the shock absorber.

Overall, the project met all objectives. The internal reaction forces were correctly solved, analytical predictions aligned with simulation results, and a careful analysis of how different aspects of the design affect suspension performance was done. The validated lower arm model accurately depicts the scenario and can be used to further validate and optimize the rear suspension system.

XII References

References

- [1] Colorado School of Mines, “*MEGN 324: Final Project Instructions*”, 2025.
- [2] SolidWorks, “*SolidWorks Simulation Documentation*”, SolidWorks 2025.
- [3] ASM International, “*Standard Material Property Tables*”, ASM Handbook, 2025.

Appendix

A.1 Assembly and Dimensions

Extra Figures of the Assembly and Relevant Dimensions

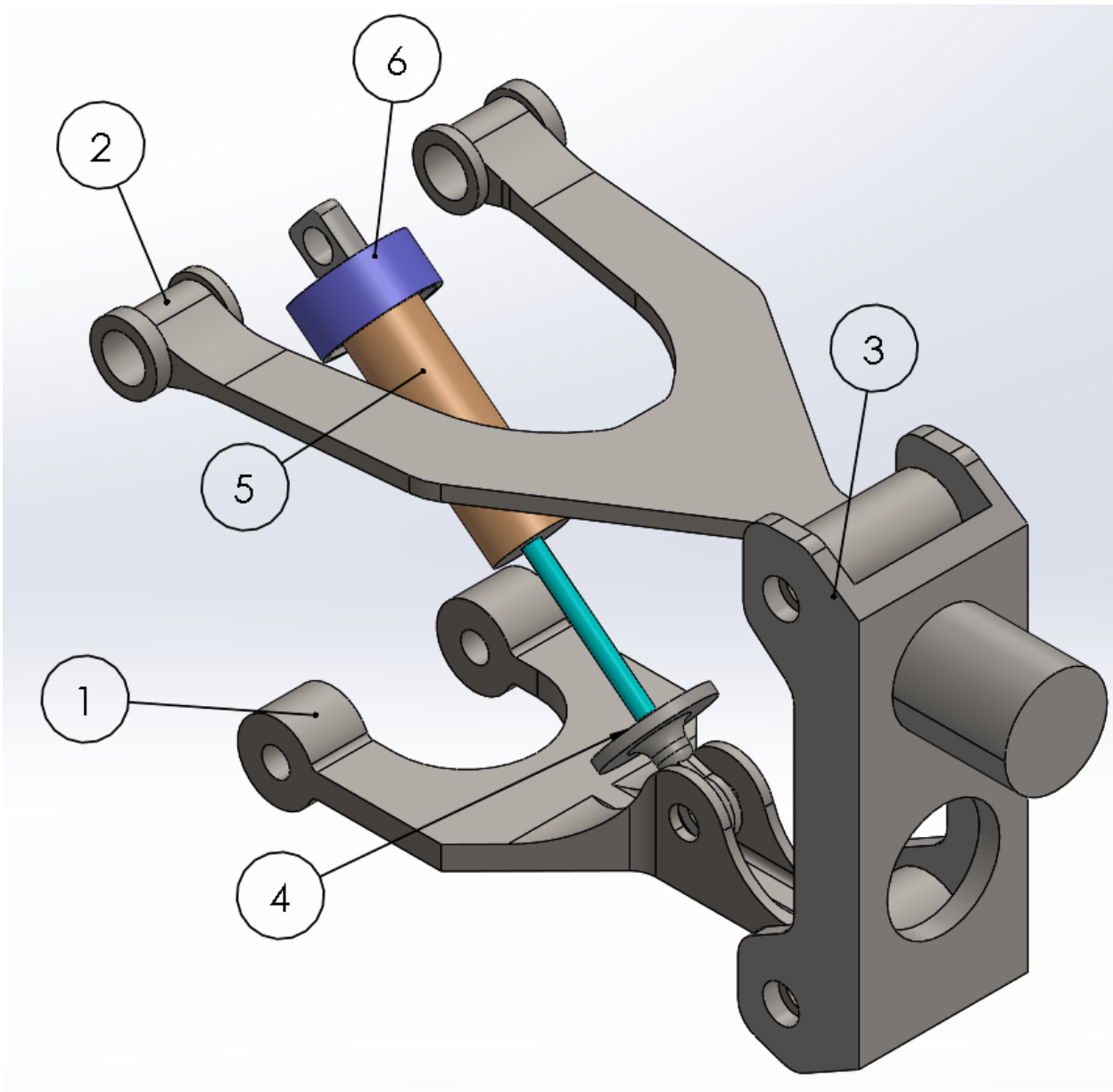


Figure 6: Rear suspension assembly.

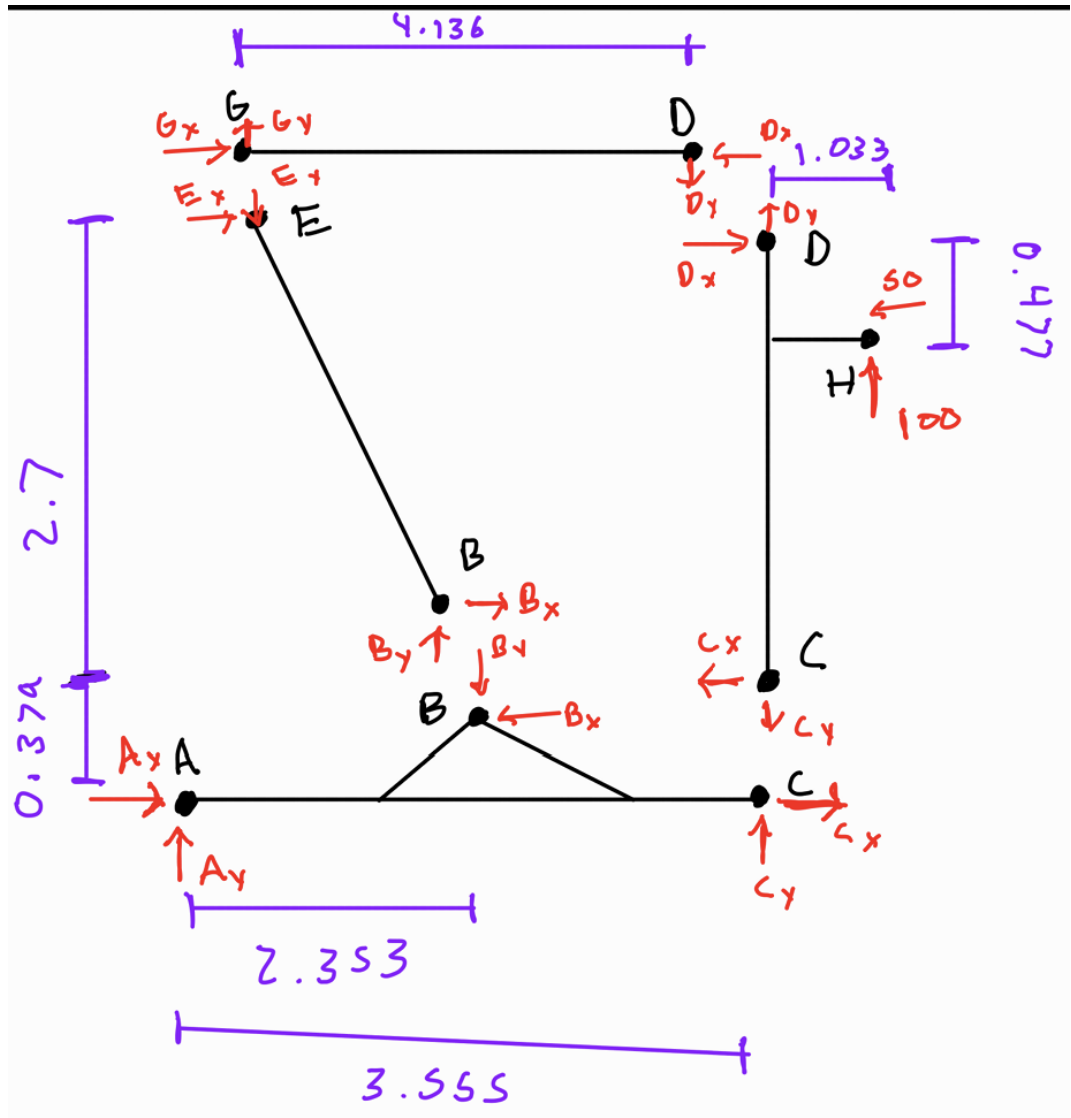


Figure 7: Free body diagram of the rear suspension statics model

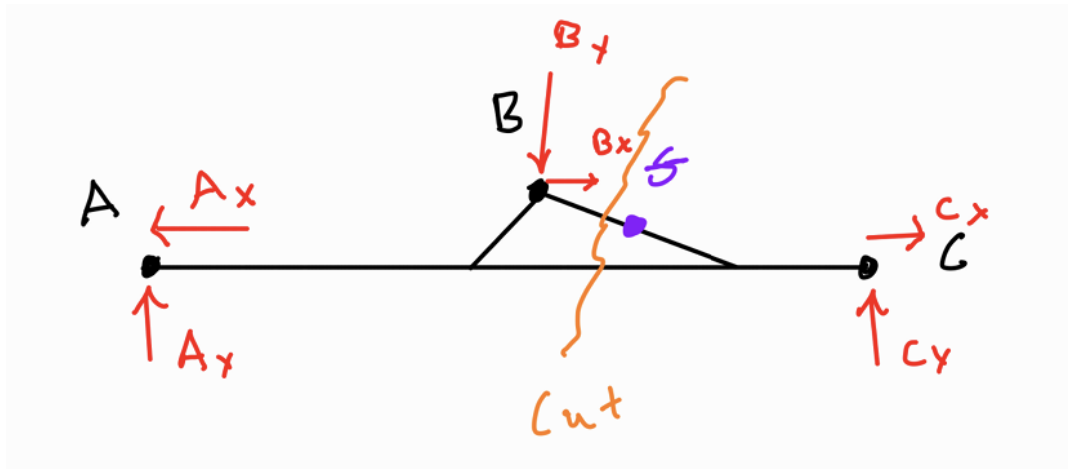


Figure 8: Free body diagram of the lower arm with internal forces with an applied section cut.

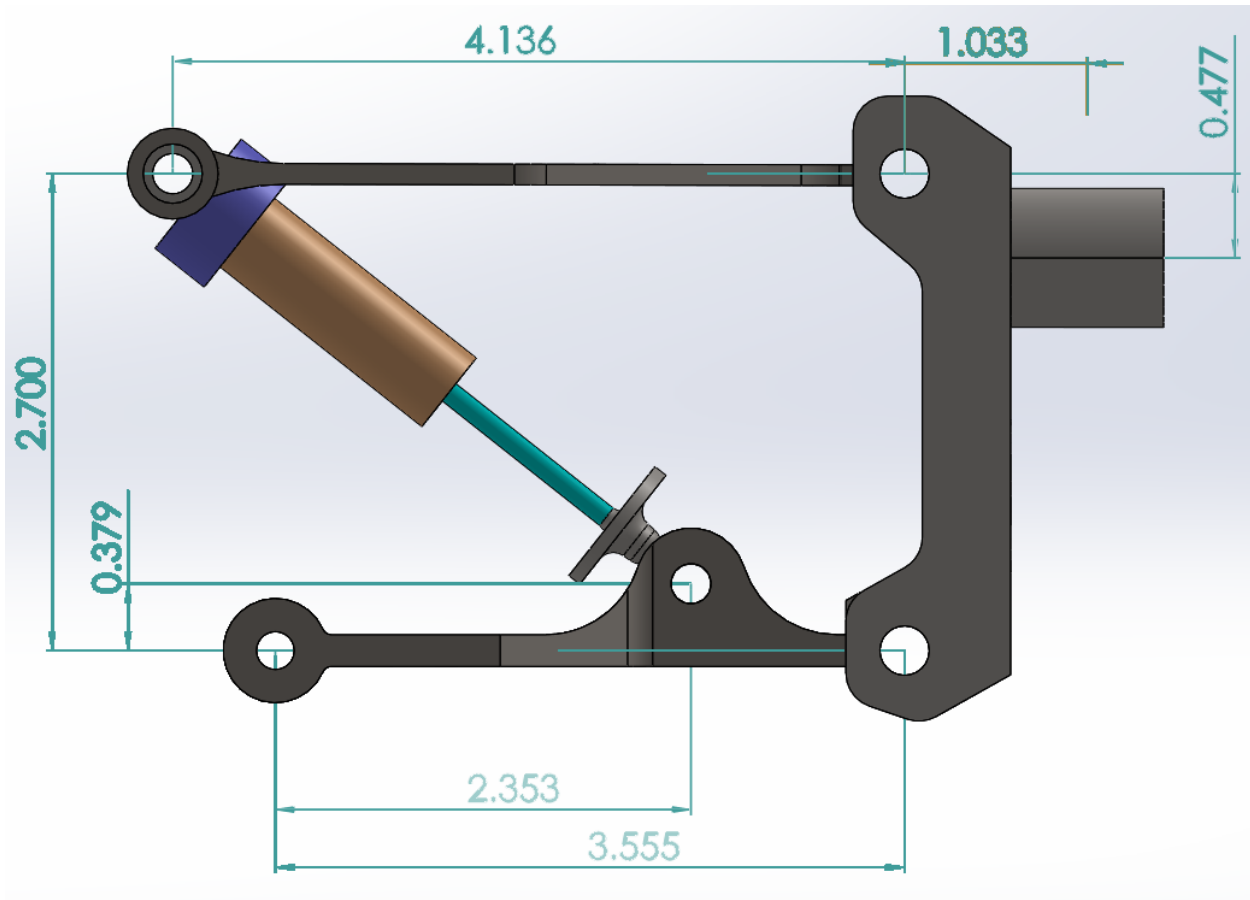


Figure 9: Key geometric dimensions.

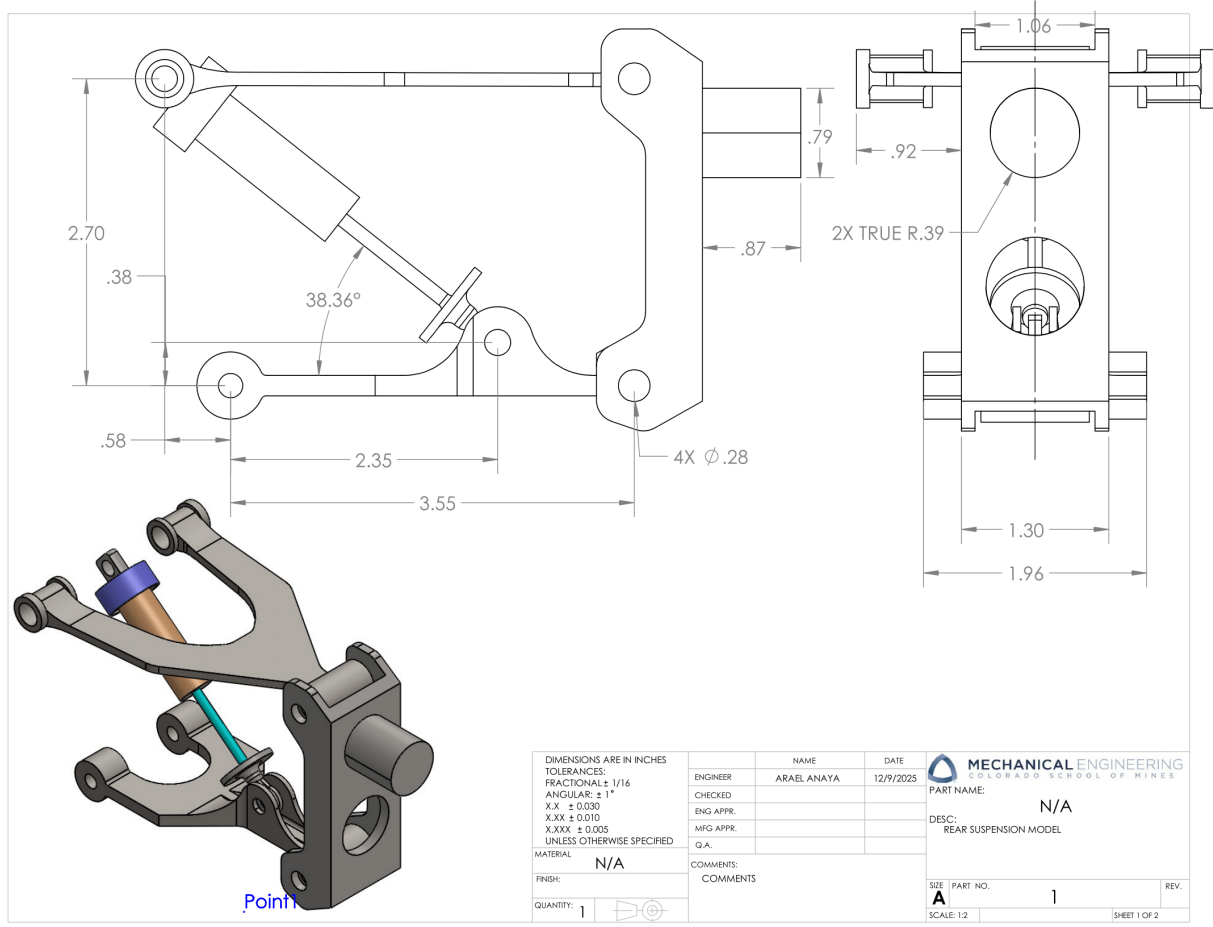


Figure 10: Engineering drawing of the complete rear suspension assembly including major dimensions

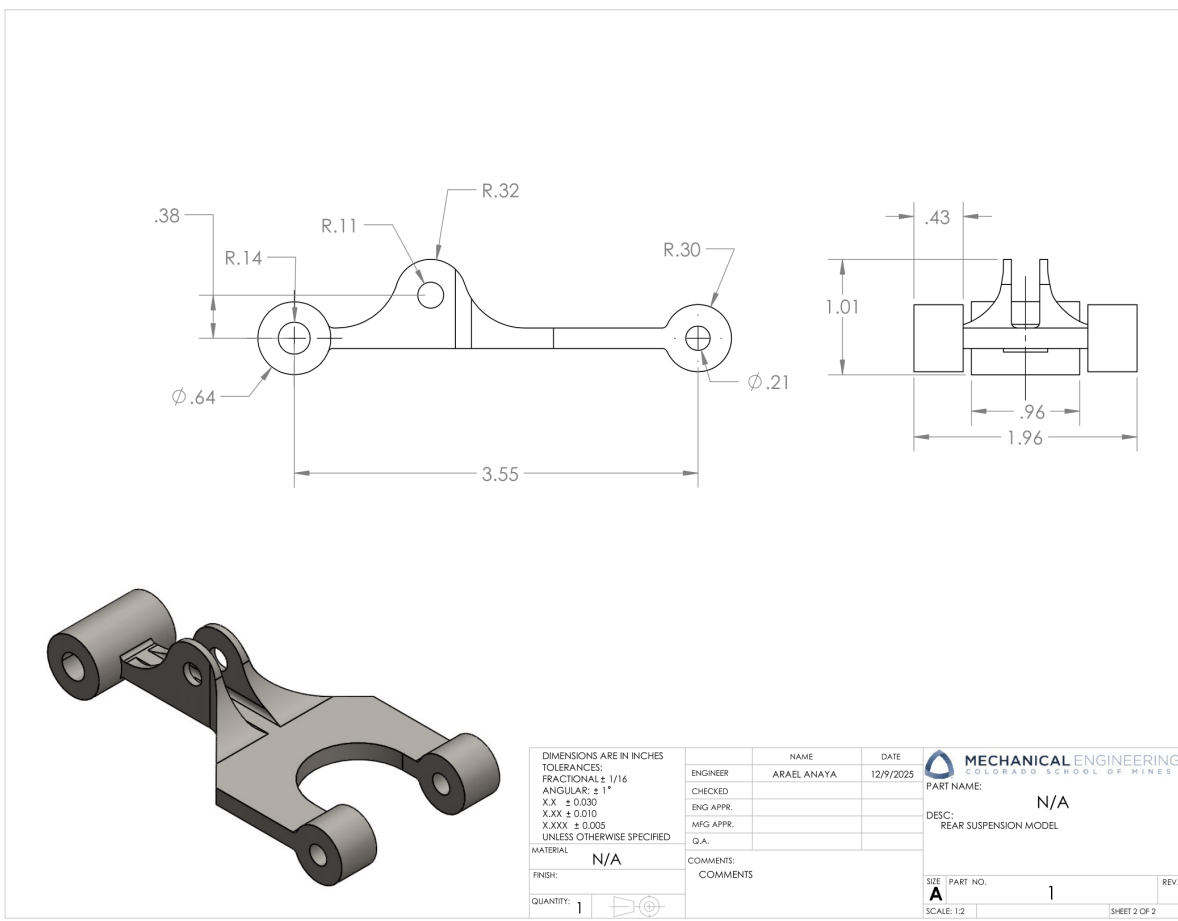
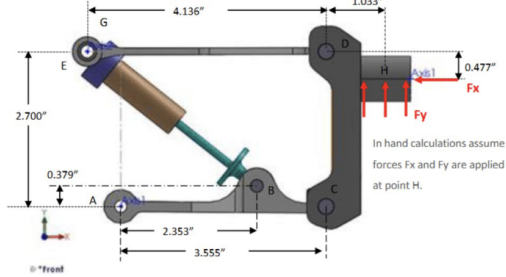


Figure 11: Engineering drawing of the lower control arm showing major dimensions and geometry.

A.2 Statics Calculations

Arael Anaya
MEGN324
Final Project Mathcad Calculations

ORIGIN := 1



$$F := \begin{bmatrix} 100 \\ 50 \end{bmatrix} \text{ lbf} \quad Px := \begin{bmatrix} 2.353 \\ 3.555 \\ 4.136 \\ 1.033 \end{bmatrix} \text{ in} \quad Py := \begin{bmatrix} .379 \\ 2.7 \\ .477 \end{bmatrix} \text{ in}$$

$$\frac{M_E}{M_D} \quad C := \begin{bmatrix} Cy \cdot Px_3 + Cx \cdot Py_2 + F_2 \cdot (Px_3 + Px_4) - F_1 \cdot Py_3 = 0 \\ Cx \cdot Py_2 + F_2 \cdot Px_4 - F_1 \cdot Py_3 = 0 \end{bmatrix} \xrightarrow{\text{solve}, Cx, Cy} [-1.462962962962963 \cdot ll]$$

$$C := \begin{bmatrix} C_{1,1} \\ C_{1,2} \end{bmatrix} = \begin{bmatrix} -1.46296 \\ -50 \end{bmatrix} \text{ lbf} \quad \theta := \text{atan} \left(\frac{Py_2 - Py_1}{Px_1 + (Px_3 - Px_2)} \right) = 38.34647 \text{ deg}$$

$$\frac{M_B}{Fx} \quad A := \begin{bmatrix} Ax \cdot Py_1 - Ay \cdot Px_1 - C_1 \cdot Py_1 - C_2 \cdot (Px_2 - Px_1) = 0 \\ Ax - F_{BE} \cdot \cos(\theta) - C_1 = 0 \\ Ay + F_{BE} \cdot \sin(\theta) - C_2 = 0 \end{bmatrix} \xrightarrow{\text{solve}, Ax, Ay, F_{BE}} \dots$$

$$F_{BE} := A_{1,3} = -101.16233 \text{ lbf} \quad A := \begin{bmatrix} A_{1,1} \\ A_{1,2} \end{bmatrix} = \begin{bmatrix} -80.80189 \\ 12.76266 \end{bmatrix} \text{ lbf}$$

$$B := \begin{bmatrix} F_{BE} \cdot \cos(\theta) \\ -F_{BE} \cdot \sin(\theta) \end{bmatrix} = \begin{bmatrix} -79.33893 \\ 62.76266 \end{bmatrix} \text{ lbf}$$

$$D := \begin{bmatrix} Dx + C_1 - F_1 = 0 \\ Dy + C_2 + F_2 = 0 \end{bmatrix} \xrightarrow{\text{solve}, Dx, Dy} [1.462962962962963 \cdot \text{lbf} + 100.0 \cdot \text{lbf} \ 50.0 \cdot \text{lbf} - 50.0 \cdot \text{lbf}]$$

$$D := \begin{bmatrix} D_{1,1} \\ D_{1,2} \end{bmatrix} = \begin{bmatrix} 101.46296 \\ 0 \end{bmatrix} \text{ lbf} \quad E := -B = \begin{bmatrix} 79.33893 \\ -62.76266 \end{bmatrix} \text{ lbf} \quad G := -D = \begin{bmatrix} -101.46296 \\ 0 \end{bmatrix} \text{ lbf}$$

Non-Commercial Use Only

Figure 12: Mathcad Statics Calculations.

Table 3: Internal forces on rear suspension parts at points A–G (magnitudes, in lbf).

| | A | B | C | D | E | G |
|-------|----------|----------|----------|-----------|----------|-----------|
| F_x | 80.8019 | 79.3389 | 1.46296 | 101.46296 | 79.3389 | 101.46296 |
| F_y | 12.7627 | 62.7627 | 50.0000 | 0.0000 | 62.7627 | 0.00000 |

For Lower Arm SWS:

$$C_{res} := \sqrt{C_1^2 + C_2^2} = 50.0214 \text{ lbf} \quad B_{res} := \sqrt{B_1^2 + B_2^2} = 101.16233 \text{ lbf}$$

$$C_{angle} := \tan\left(\frac{-C_2}{-C_1}\right) = 88.32405 \text{ deg} \quad B_{angle} := \tan\left(\frac{B_2}{B_1}\right) = -38.34647 \text{ deg}$$

Figure 13: Calculation of resultant forces and corresponding application angles for the lower arm split-lines.

Arael Anaya
MEGN324
Final Project Mathcad Calculations

Case 1:

$$L_{shock} := \begin{bmatrix} 2.711 \\ 1.215 \end{bmatrix} \text{ in} \quad d_{shock} := \begin{bmatrix} .4961 \\ .3961 \\ .1248 \end{bmatrix} \text{ in} \quad Area := \begin{bmatrix} \frac{1}{4} \cdot \pi \cdot (d_{shock_1}^2 - d_{shock_2}^2) \\ \frac{1}{4} \pi \cdot (d_{shock_3})^2 \end{bmatrix} = \begin{bmatrix} 0.07007 \\ 0.01223 \end{bmatrix} \text{ in}^2$$

$$E := \begin{bmatrix} 200000 \\ 200000 \end{bmatrix} \text{ MPa} \quad K := \begin{bmatrix} \frac{E_1 \cdot Area_1}{L_{shock_1} - L_{shock_2}} \\ \frac{E_2 \cdot Area_2}{L_{shock_2}} \end{bmatrix} \quad F := F_{BE} = -101.16233 \text{ lbf}$$

$$u := \frac{F}{\left(\frac{1}{K_1} + \frac{1}{K_2} \right)^{-1}} = -0.00042 \text{ in} \quad \text{Springs in Series}$$

$$u_1 := \frac{F}{K_1} = -0.00007 \text{ in} \quad u_2 := \frac{F}{K_2} = -0.00035 \text{ in} \quad u_1 + u_2 = -0.00042 \text{ in}$$

Case 2:

$$K_s := 500 \frac{\text{lbf}}{\text{in}} \quad \frac{F}{K_s} = -0.20232 \text{ in}$$

For Lower Arm SWS:

$$C_{res} := \sqrt{C_1^2 + C_2^2} = 50.0214 \text{ lbf} \quad B_{res} := \sqrt{B_1^2 + B_2^2} = 101.16233 \text{ lbf}$$

$$C_{angle} := \tan \left(\frac{-C_2}{-C_1} \right) = 88.32405 \text{ deg} \quad B_{angle} := \tan \left(\frac{B_2}{B_1} \right) = -38.34647 \text{ deg}$$

Non-Commercial Use Only

Figure 14: Mathcad Spring Calculations.

Arael Anaya
MEGN324
Final Project Mathcad Calculations

Lower Arm Stress Calculation

$$C := -C = \begin{bmatrix} 1.46296 \\ 50 \end{bmatrix} \text{ lbf}$$

$$\begin{aligned} S_1 &:= C_1 + S_x = 0 \xrightarrow{\text{solve}, S_x} -1.462962962962963 \cdot \text{lbf} \\ S_2 &:= C_2 + S_y = 0 \xrightarrow{\text{solve}, S_y} -50.0 \cdot \text{lbf} \end{aligned}$$

$$S = \begin{bmatrix} -1.46296 \\ -50 \end{bmatrix} \text{ lbf} \quad S_{mag} := \sqrt{S_1^2 + S_2^2} = 50.0214 \text{ lbf}$$

$$Px = \begin{bmatrix} 2.353 \\ 3.555 \\ 4.136 \\ 1.033 \end{bmatrix} \text{ in} \quad Py = \begin{bmatrix} 0.379 \\ 2.7 \\ 0.477 \end{bmatrix} \text{ in} \quad Ps := \begin{bmatrix} 3 \\ .12 \end{bmatrix} \text{ in}$$

$$M_s := C_1 \cdot Ps_2 + C_2 \cdot (Px_2 - Ps_1) + M_s = 0 \xrightarrow{\text{solve}, M_s} -27.925555555555555556 \cdot \text{in} \cdot \text{lbf}$$

$$M_s = -27.92556 \text{ lbf} \cdot \text{in}$$

$$a := 0.19 \text{ in} \quad b := 0.4 \text{ in} \quad Area_s := a \cdot b \quad C_s := \frac{a}{2} \quad I_s := \frac{1}{12} \cdot a^3 \cdot b = 0.00023 \text{ in}^4$$

$$\sigma_{axial} := \frac{S_1}{Area_s} = -0.01925 \text{ ksi} \quad \sigma_{bending} := \frac{M_s \cdot C_s}{I_s} = -11.60342 \text{ ksi}$$

$$\sigma := \sigma_{axial} + \sigma_{bending} = -11.62267 \text{ ksi}$$

Non-Commercial Use Only

Figure 15: Mathcad Lower Arm Stress Calculations.

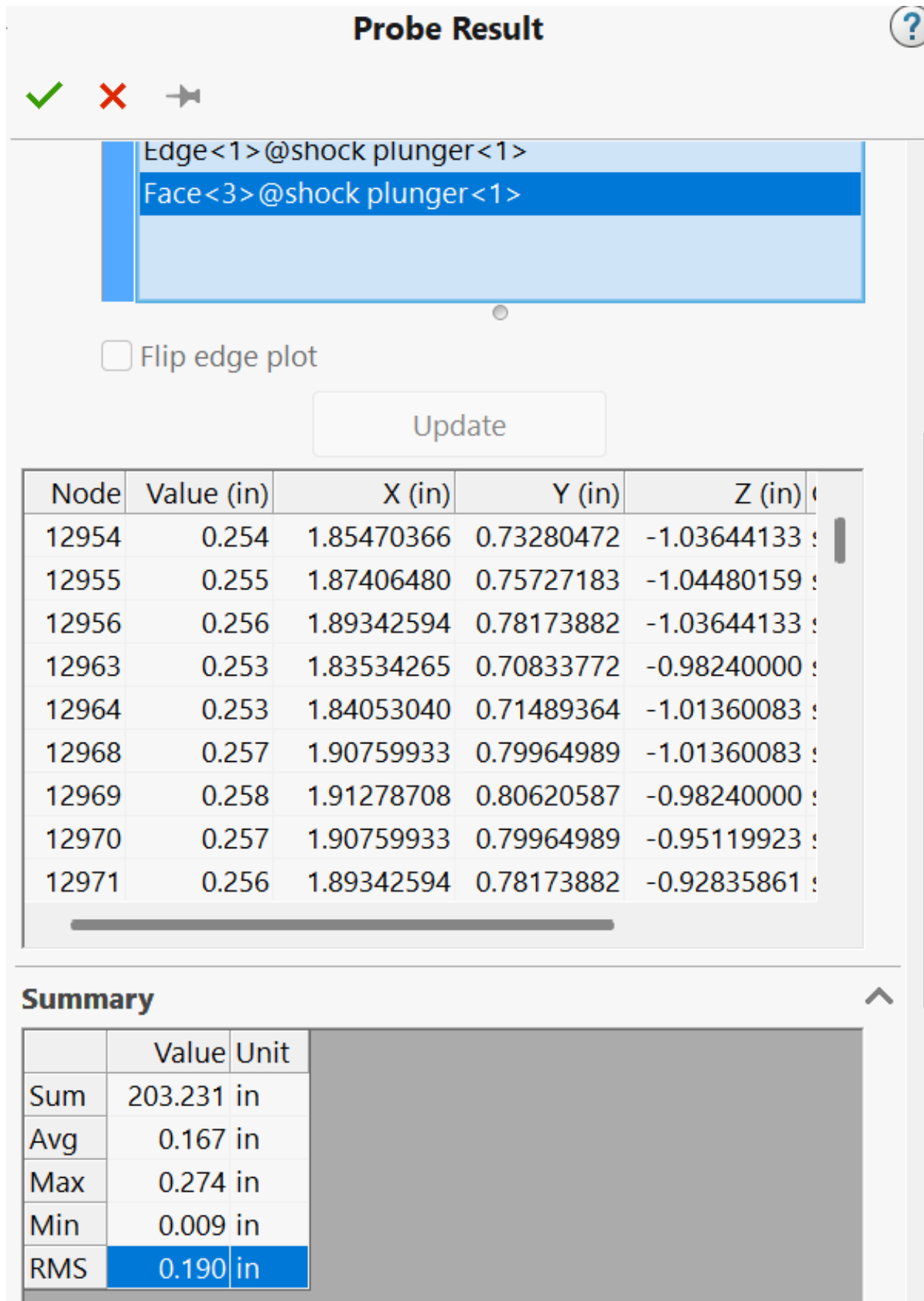


Figure 16: Resultant Displacement Probe of study 2.

A.3 FEA Mesh Details

Includes mesh screenshots, convergence tables, and any other relevant info.

Table 4: Mesh convergence results for the lower arm study.

| Element Size h (in) | 1/ h | Max Von Mises (ksi) | % Difference |
|-----------------------|--------|----------------------|--------------|
| 0 (no control) | 0 | 17.747 | — |
| 0.05000 | 20 | 18.799 | -5.76% |
| 0.02500 | 40 | 19.087 | -1.52% |
| 0.01250 | 80 | 19.506 | -2.17% |
| 0.00625 | 160 | 7.9054×10^6 | -199.90% |

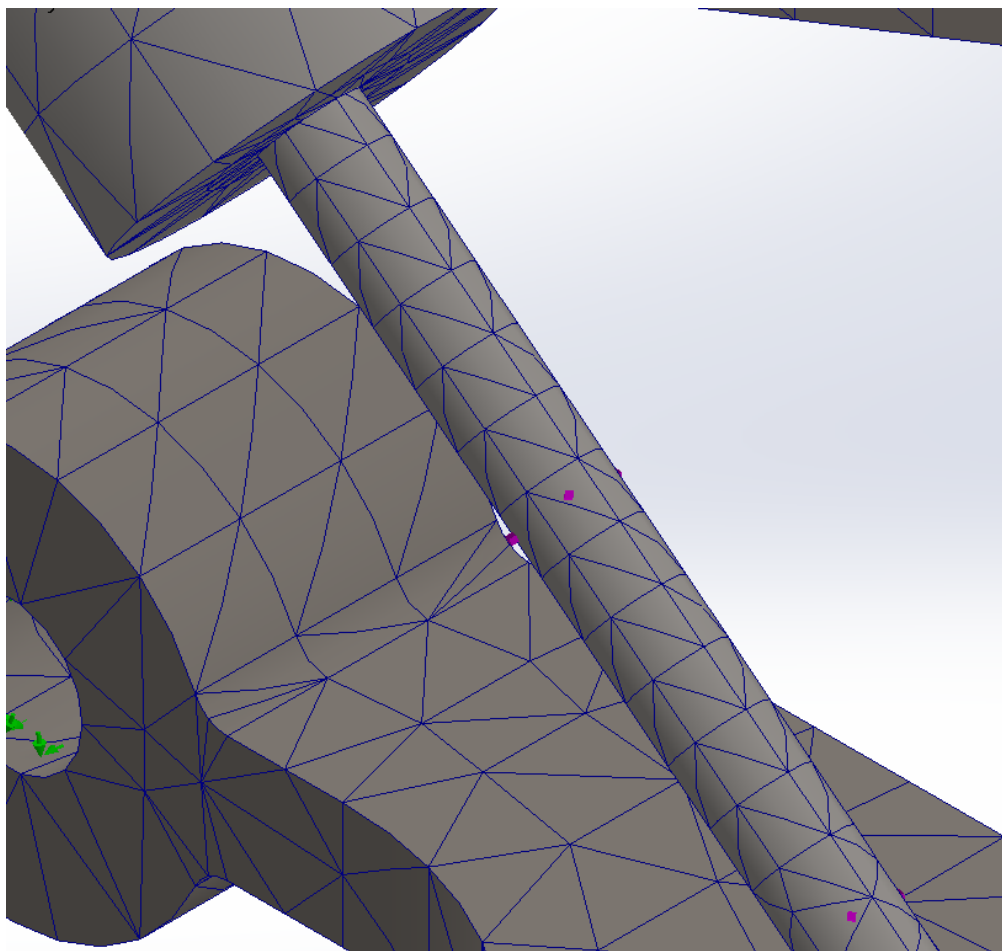


Figure 17: Closeup of Mesh Control applied to plunger tube section.

A.4 SolidWorks Simulations Configuration

SolidWorks Simulation Configuration Settings

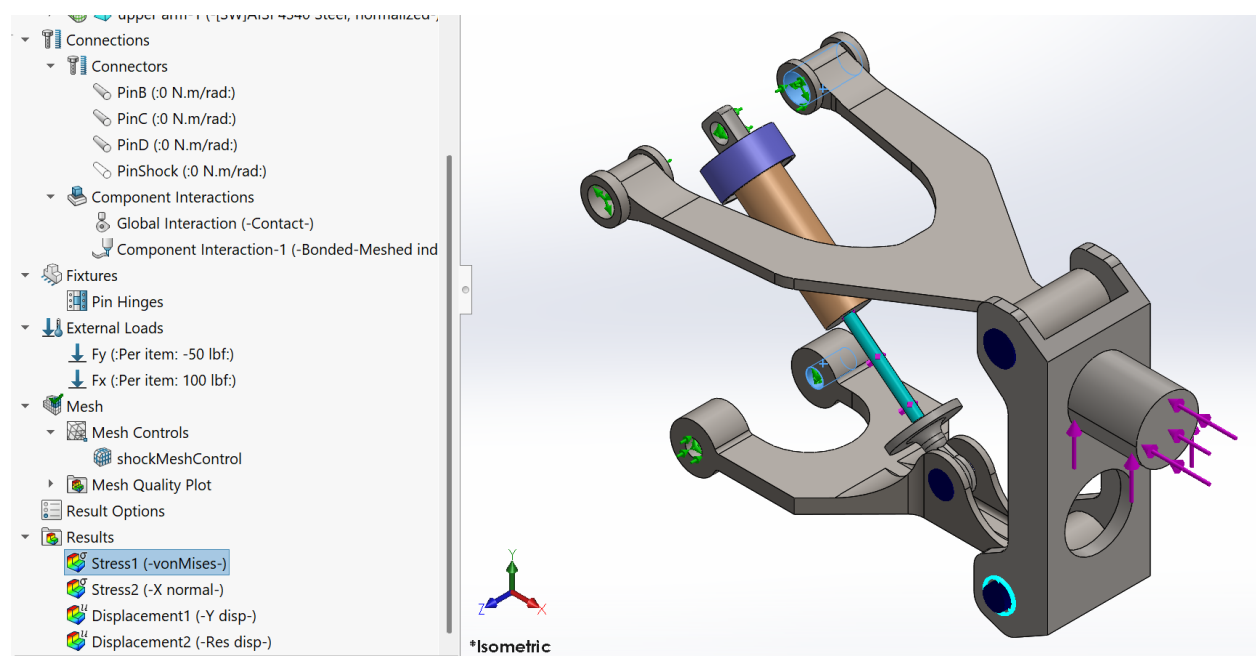


Figure 18: Simulation configuration for project assembly.

A.5 FEA Result Details

Includes additional Results for Von Mises analysis that did not fit inside of main report.

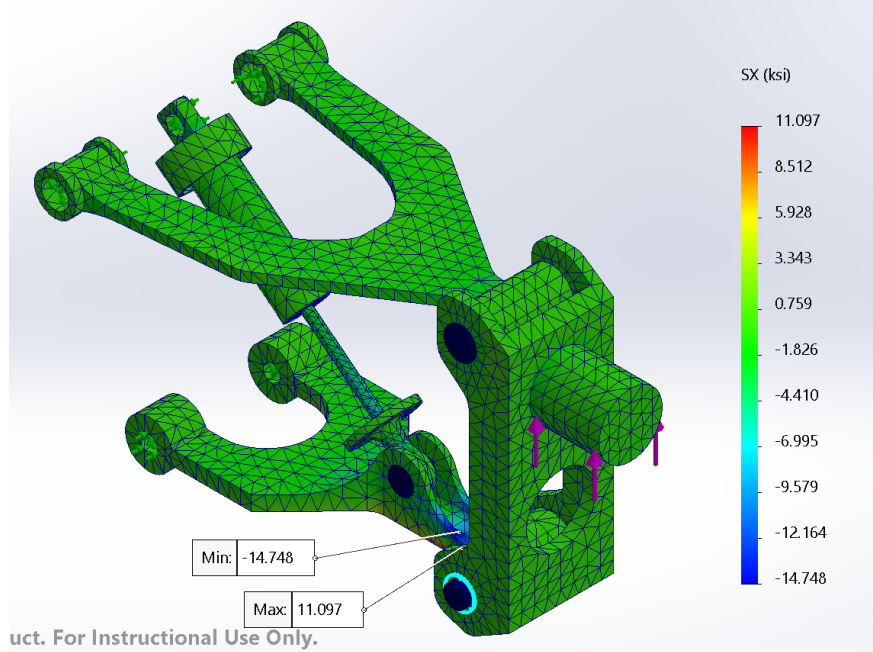


Figure 19: Study 1: σ_x (X-direction) stress distribution.

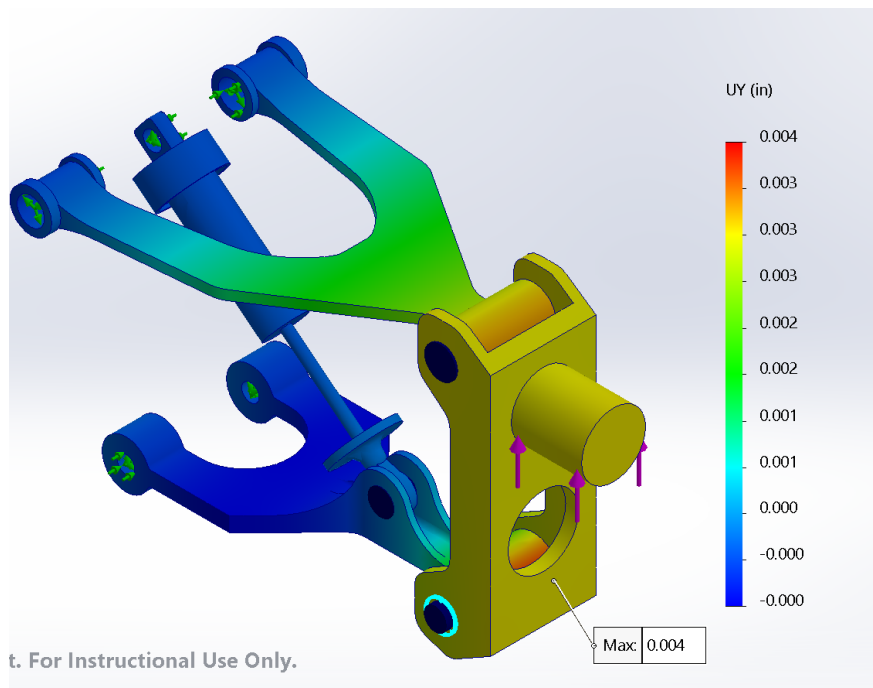


Figure 20: Study 1: Y-direction displacement contour.

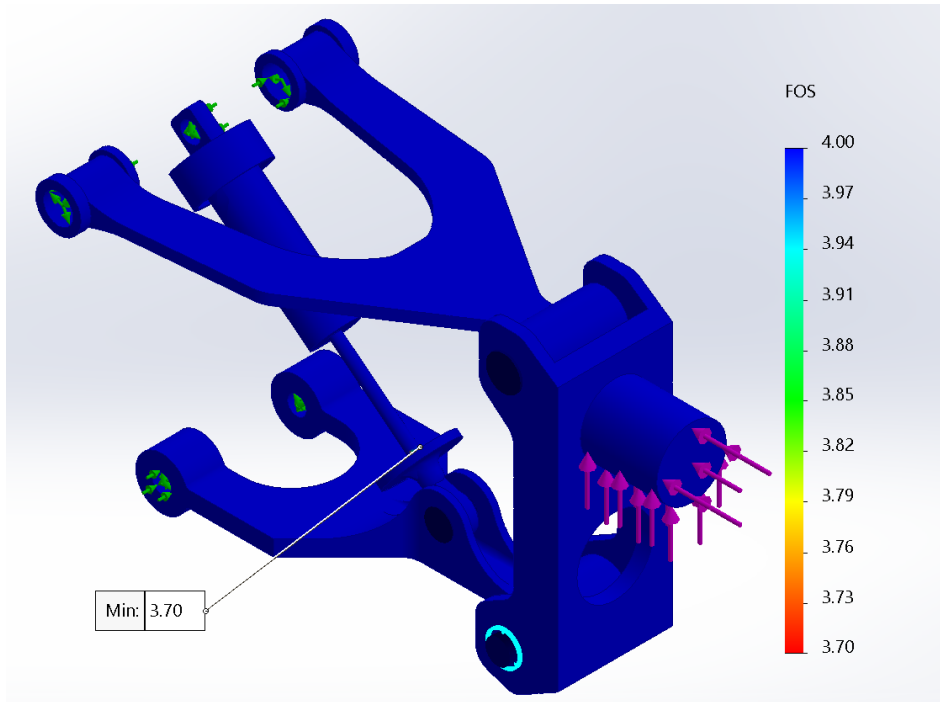


Figure 21: Factor of Safety contour plot for Study 1 (fixed shock configuration). Minimum FOS occurs at the lower arm fillet region.

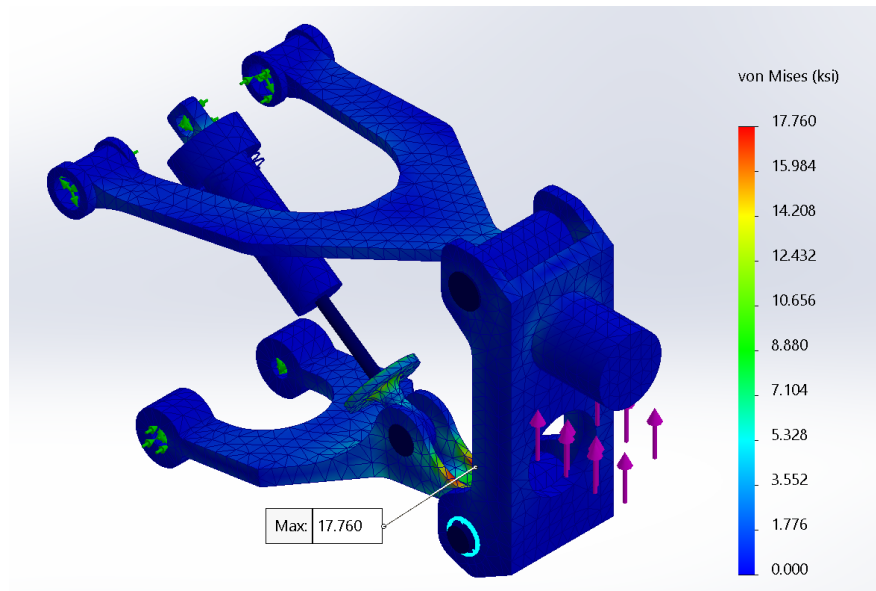


Figure 22: Study 2: Von Mises stress distribution for spring-supported shock.

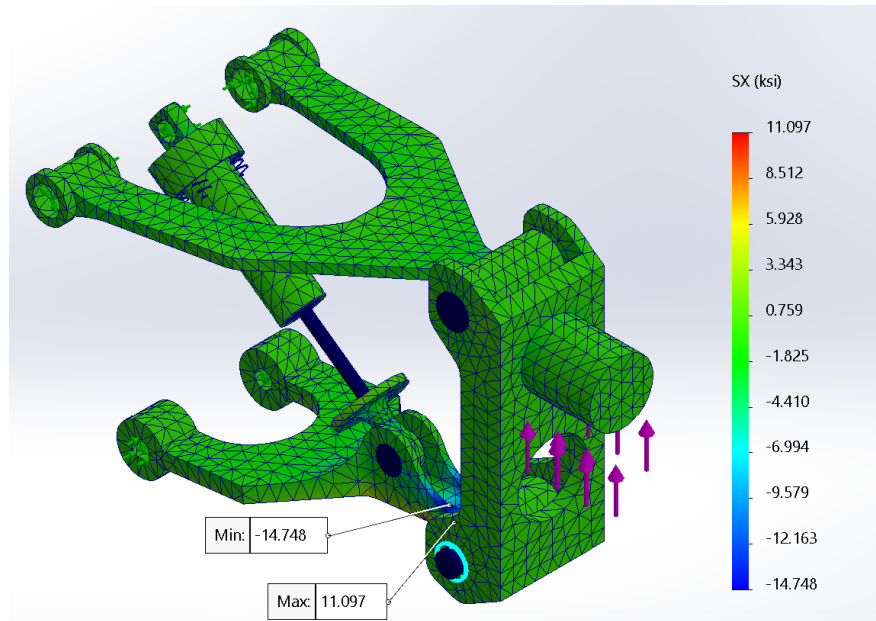


Figure 23: Study 2: σ_x (X-direction) stress distribution.

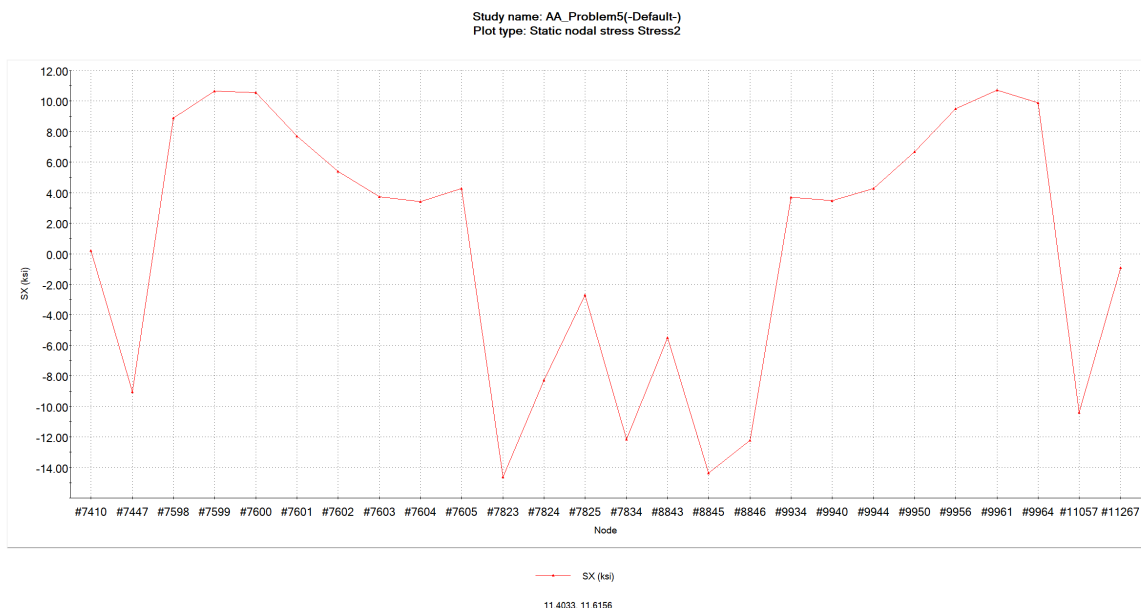


Figure 24: Static nodal stress distribution (S_x in ksi) along the selected edge for Study 2.

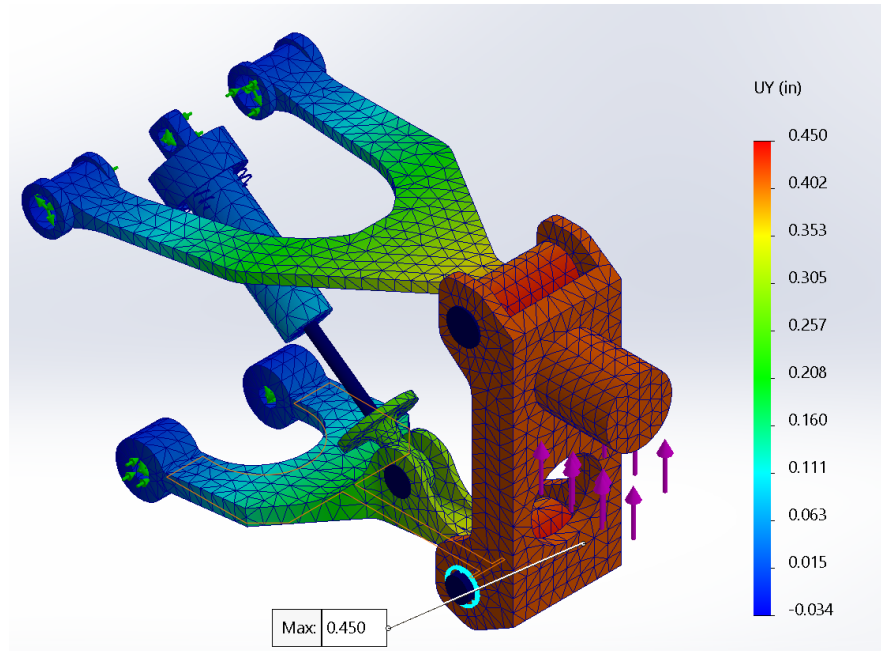


Figure 25: Study 2: Y-direction displacement contour.

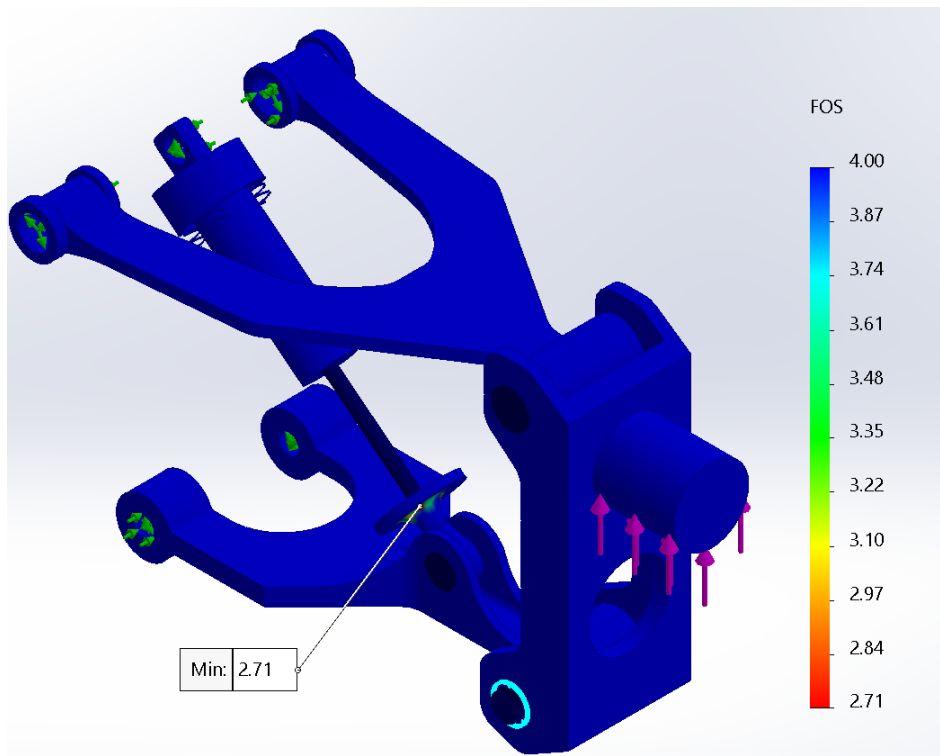


Figure 26: Factor of Safety contour plot for Study 2 (spring-supported shock). Reduced stiffness results in a lower minimum FOS compared to Study 1.

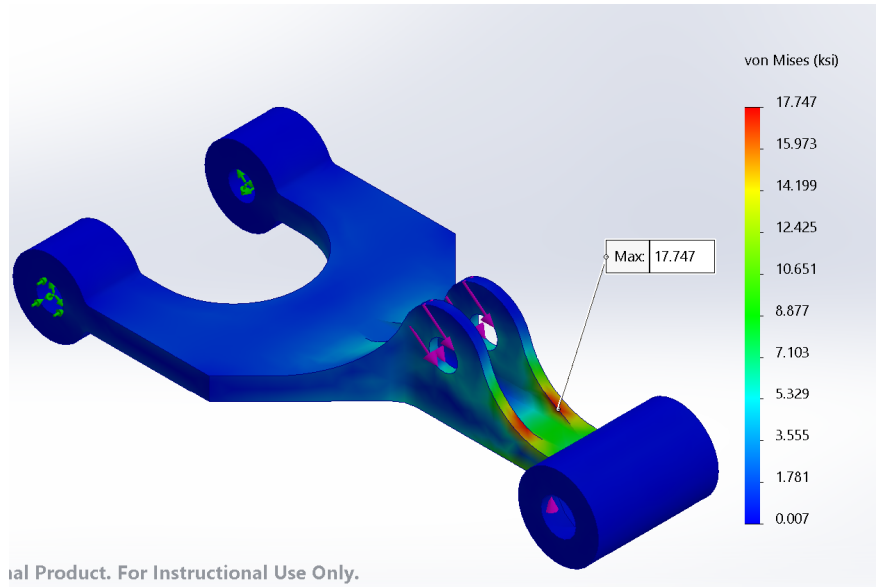


Figure 27: Study 3: Converged Von Mises stress distribution for lower arm model.

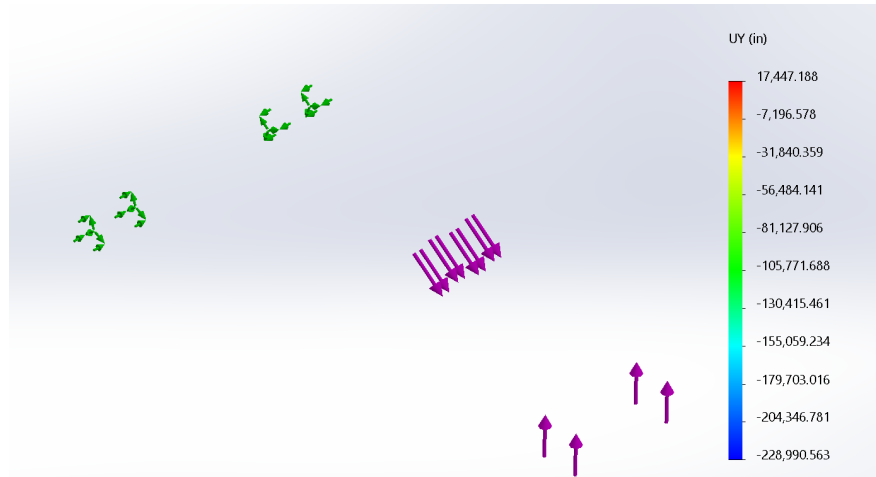


Figure 28: Study 3: Y-direction displacement field (view A).

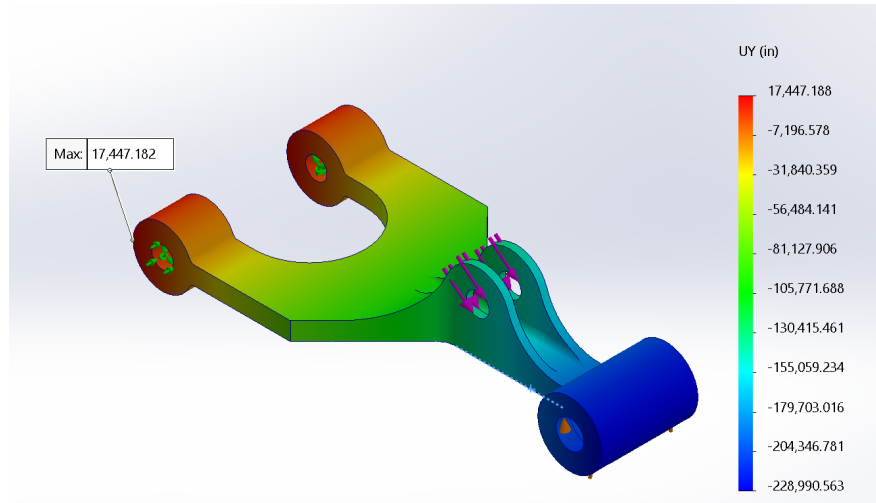


Figure 29: Study 3: Y-direction displacement field (view B).

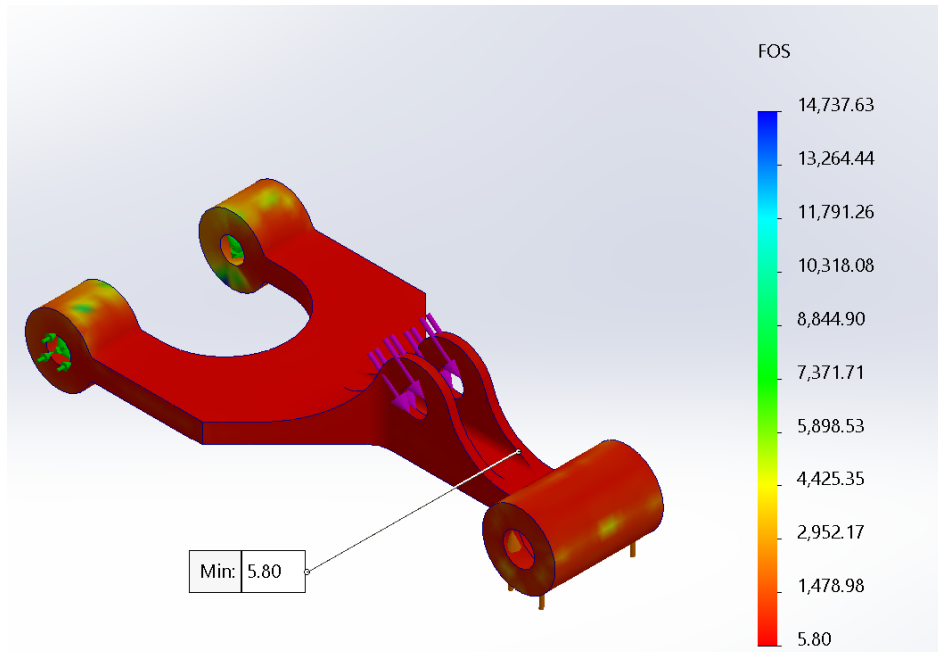


Figure 30: Factor of Safety contour plot for Study 3 (lower arm only model). Minimum FOS localized at the inner fillet region near the applied reactions.

A.6 FEA Design Study Details

Includes additional Results for lower arm design study analysis that did not fit inside of main report.

Variables

| | | | |
|---|-------|---------------|---------------|
| dv1a | Range | Min: 0.250000 | Max: 0.270000 |
| dv2a | Range | Min: 0.130000 | Max: 0.180000 |
| Click here to add Variables | | | |

Constraints

| | | | |
|---|-----------------|---------------|----------|
| Minimum Factor of Safety1 | is greater than | Min: 3.500000 | AA_Stati |
| Click here to add Constraints | | | |

Goals

| | |
|---|----------|
| Volume2 | Minimize |
| Click here to add Goals | |

Figure 31: Design study setup showing variable ranges, minimum Factor of Safety constraint, and volume minimization goal.

Table 5: Design study iteration results for lower arm optimization.

| Parameter | Current | Initial | Optimal | Iter. 1 | Iter. 2 | Iter. 3 | Iter. 4 | Iter. 5 | Iter. 6 | Iter. 7 | Iter. 8 | Iter. 9 |
|---------------------------|---------|---------|---------|---------|----------|---------|---------|---------|---------|---------|---------|---------|
| Gap | 0.25 | 0.25 | 0.25 | 0.27 | 0.25 | 0.27 | 0.25 | 0.27 | 0.25 | 0.26 | 0.26 | 0.26 |
| Base | 0.13 | 0.18 | 0.13 | 0.18 | 0.180000 | 0.13 | 0.13 | 0.15 | 0.15 | 0.18 | 0.13 | 0.15 |
| Minimum FOS | 3.523 | 5.525 | 3.523 | 5.152 | 5.525 | 3.146 | 3.523 | 4.139 | 4.505 | 5.416 | 3.308 | 4.317 |
| Volume (in ³) | 0.87 | 1.00 | 0.87 | 0.99 | 1.00 | 0.86 | 0.87 | 0.93 | 0.93 | 1.00 | 0.87 | 0.93 |